J Comput Aided Mol Des (2011) 25:569–581
DOI 10.1007/s10822-011-9442-0

Application of shape-based and pharmacophore-based in silico screens for identification of Type II protein kinase inhibitors

Daniel Mucs · Richard A. Bryce · Pascal Bonnet

Received: 20 January 2011 / Accepted: 1 June 2011 / Published online: 17 June 2011

Abstract The identification of new, potent and selective inhibitors of important protein kinase targets is a major goal of drug discovery. Here we analyze the crystal structures of 55 protein kinase complexes with Type II inhibitors and find they adopt a conserved twisted V-shape, with an angle of 121 ± 8° and twist of 78 ± 8°. The tightly conserved twist appears important in ensuring ligands curve around the protein backbone and towards the deep pocket. From this, we develop predictive pharmacophore- and shape-based screens to identify Type II inhibitors from a database which also contains Type I inhibitors as decoys. Both approaches exhibit a good level of discrimination for Type II molecules. The most effective pharmacophore model requires six features and three excluded volume regions. Shape-based screening using ROCS generally performs at least as well as pharmacophore approaches. There is only a moderate dependence of shape-based or pharmacophore-based screens on the underlying conformer generator (MOE, Macromodel, Omega and SPE), as well as on ligand linkage chemistry (amide and urea). Finally, we apply our approach to retrieval of Type II inhibitors from a modified version of the DUD database, containing over 104,000 compounds. We observe good enrichment, providing further evidence that the in silico screens developed here will constitute useful guides for identification of small molecule inhibitors targetting protein kinases in their inactive conformational state.

Keywords Type II kinase inhibitors · Virtual screening · Pharmacophore · ROCS · Shape-based screening

Electronic supplementary material The online version of this article (doi:10.1007/s10822-011-9442-0) contains supplementary material, which is available to authorized users.

D. Mucs · R. A. Bryce (✉)
School of Pharmacy and Pharmaceutical Sciences, University of Manchester, Oxford Road, Manchester M13 9PT, UK
e-mail: r.a.bryce@manchester.ac.uk

P. Bonnet (✉)
Pharmaceutical Research & Development, A Division of Janssen Pharmaceutica N.V., Johnson & Johnson, Turnhoutseweg 30, 2340 Beerse, Belgium
e-mail: pbonnet@its.jnj.com

Introduction

Protein kinases are one of the major drug targets of today, due to their central role in regulation of human physiology. There are approximately 500 protein kinases in the human genome, linked with a great variety of signal transduction processes through a phosphorylation cascade [1]. Dysfunction of protein kinases can be linked with several diseases, including cancer, diabetes, inflammation, cardiovascular disorders and infectious diseases [2]. Inhibition of specific protein kinases is therefore of great potential therapeutic benefit. In developing protein kinase therapeutics, however, specificity and selectivity are major problems, as protein kinases share a common structural fold and catalytic mechanism. This reflects their dependence on ATP, an essential cofactor that contributes its γ-phosphate during protein kinase catalysis.

Consequently, there are a number of conserved structural elements among protein kinases, in particular around the catalytic domain and ATP binding site. The non-conserved regions are often loop features [3]. The common active site structure of protein kinases has been well characterized crystallographically [1]. The catalytic unit contains two major domains (N- and C-terminal) and

within them a further 11 subdomains [4]. The two major domains are linked by a hinge region which permits rotation of domains relative to one another in the event of binding ATP or substrate [4]. Most protein kinases require phosphorylation on one or more of the Ser, Thr or Tyr residues situated on the activation loop. This phosphorylation leads to conformational change in the protein, enabling substrate binding and catalytic residues to shift into an active orientation. The ATP binding site is located between the two major domains; binding of the ATP molecule occurs via a number of hydrogen bonds to the divalent cation cofactor and the enzyme. Type I protein kinase inhibitors bind to the ATP binding site of protein kinases, generally to the hinge region. They are ATP competitive and require high binding affinity to compete with the high in vivo concentration of ATP ($\sim$mM). Binders in this hinge region usually have hydrogen donor and acceptor groups, forming at least one hydrogen bond [5]. Because of the commonality of this site and its details, it has proved difficult to ensure inhibitor selectivity, although the design of some selective Type I inhibitors has been successful [5].

In the vicinity of the ATP binding site is the protein kinase's DFG (Asp-Phe-Gly) motif. This DFG motif is located at the start of the activation loop and plays an essential role in catalysis. The motif is very well conserved in almost all protein kinases, although sometimes Phe is replaced by Leu, Tyr or Trp [4]. In the inactive protein kinase state, a distinct "DFG-out" conformation [6] is adopted (Fig. 1a): Phe rotates away from a nearby helix (the αC helix) and projects into the ATP pocket. As a result, a novel hydrophobic cavity is exposed, often referred to as the hydrophobic, allosteric or deep pocket [7]. In the active form of the protein kinase, the "DFG-in" motif conformation is present (Fig. 1b) [8]. In this case, access to the deep pocket is hindered. Structural rearrangement of the DFG motif, as well as the αC helix, is evident on activation. Another loop, termed the glycine-rich loop plays an essential role in positioning the phosphate groups of ATP during catalysis [7]. Analysis of several crystal structures reveals that the glycine-rich loop can move substantially upon binding of protein kinase inhibitors [9].

Type II inhibitors specifically exploit this DFG-out conformation, projecting into the exposed deep pocket in the inactive state of the protein kinase (Fig. 1a). Type II inhibitors usually also have a hinge binding group but it is not essential [10, 11]. Therefore, Type II inhibitors are often still ATP competitive, but target a form of the protein kinase which displays less affinity for ATP. Currently, there are far fewer Type II than Type I protein kinase inhibitors in clinical development but these compounds show in general a greater protein kinase selectivity profile [7]. Recently, we note the identification of Type I½ protein kinase inhibitors, which specifically target protein kinases in a DFG-in conformation, occupying the ATP binding site but also interacting with residues associated with Type II inhibitor design [12].

Various attempts have been made to qualitatively rationalize the broad structural features that govern Type II protein kinase inhibitor binding [5, 13–15]. For example, Backes et al. [5] resolved inhibitor features into four groups, which interact with the hinge region, the DFG loop, a Glu-Lys pair and the deep pocket. However, inspection of Type I and Type II protein kinase inhibitors suggest that the structural differences between the ligand classes are not straightforward to describe. Indeed, many Type I inhibitors appear to have a very Type II-like chemical scaffold. For example, Type II inhibitors such as imatinib **1** [16], BIRB796 **2** [11], sorafenib **3** [17] and nilotinib **4** [18] bear considerable resemblance to the Type I inhibitors such as an inhibitor of Lck protein kinase **5** [19], dasatinib **6** [20], or an inhibitor of Aurora A **7** (Scheme 1) [21]. This makes it difficult to distinguish Type I from Type II ligands; however, we note some recent success in identifying Type II inhibitors using a receptor-based approach by Kurafeva and Abagyan [6], where DFG-in kinase structures are

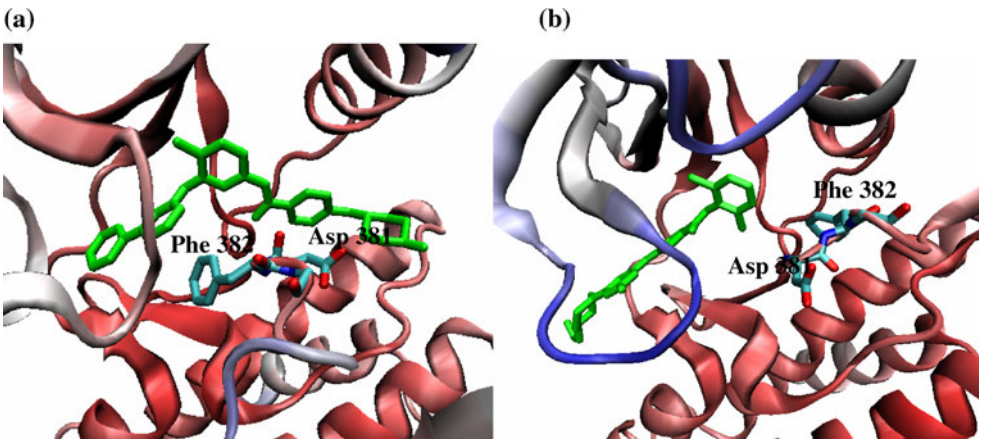

Fig. 1 **a** DFG-out conformation, with Type II inhibitor, imatinib, PDB code 1IEP; **b** DFG-in conformation, with Type I inhibitor, dasatinib, PDB code 2GQG

Scheme 1 Structure of imatinib (**1**), BIRB796 (**2**), sorafenib (**3**), nilotinib (**4**), pyrimidine amide 11 (**5**), dasatinib (**6**) and Aurora A inhibitor AK1 (**7**)

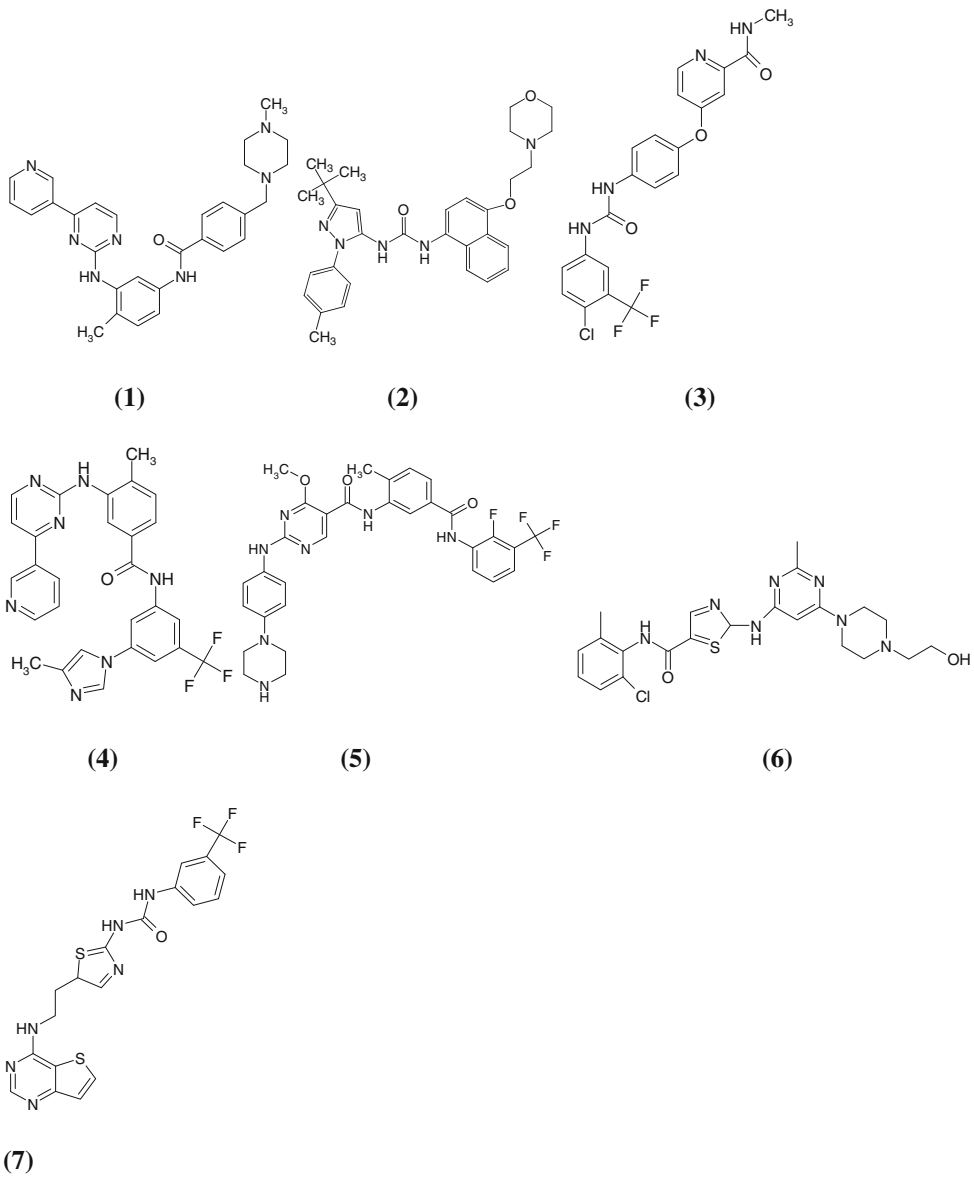

converted to putative DFG-out conformations and used in virtual screening campaigns. In this study, we present a systematic and comprehensive analysis of the crystal structures of 55 protein kinase complexes with Type II inhibitors, characterising key geometric features. We then develop a predictive strategy to specifically retrieve Type II inhibitors during a ligand-based virtual screening campaign. As a demanding control, we use a database of 83 Type I inhibitors containing Type II-like chemical features. Our ligand-based screening approach explores both pharmacophore and shape-based methods, the latter employing the volume-overlap method, ROCS (Rapid Overlay of Chemical Structures) [22]. We assess the ability of the methods to distinguish Type II from Type I inhibitors, considering also the effect of ligand protonation state and conformational search algorithm on our approaches.

Methods

Ligand libraries and conformer generation

Based on the DFG loop conformation, a set of 83 Type I and 55 Type II inhibitor/protein kinase structures were identified from the Brookhaven Protein Data Bank (Online resource, Tables 1S, 2S). Within these *Type I* and *Type II* ligand sets, we identify inhibitors with urea-based and amide-based groups between their linker and hydrophobic groups. The *Urea* set contains 8 Type I and 12 Type II ligands; the *Amide* set holds 75 Type I and 31 Type II ligands. For each of the Type I and Type II ligand sets, protonation states for N (neutral) and Z (zwitterion) sets were created using the MOE *wash* function [23]. The N set contains deprotonated basic and

protonated acidic groups. The Z set has protonated basic and deprotonated acidic groups (Fig. 1S). Then, for generating the conformational ensembles for the inhibitor databases (N and Z versions of the *Amide*, *Urea* and *Type II* sets, see below), four different conformer generators were used: Macromodel [24], MOE [23], Omega [25] and stochastic proximity embedding (SPE) [26]. Macromodel (version v95207) was used applying the Monte Carlo Multiple Minimum method with a usage-directed search. MOE (version 2008.10) used a systematic rule-based approach. Omega (version 20071130) uses a fragment reassembly approach. SPE generates conformations that satisfy a set of distance and volume constraints derived from the molecular connectivity table. Conformational boosting [27] was applied to bias the conformational search towards more extended conformations. For the four conformer generators, equivalent search parameters were set: the MMFF94s force field [28–33] was used, along with a RMSD tolerance of 0.25 Å and an energy window of 20 kcal/mol. Following Tresadern et al.'s comparative study of conformational searching algorithms [34], we use a maximum number of conformers per molecule of 1,000. As the conformer generators use different methods for creating the conformer database, different numbers of conformers arise from a given method.

The compactness of conformations generated was assessed by computing the maximum and minimum radius of gyration (using MOE descriptor *rgyr*) for all conformations of each Type II ligand, giving R_g^{max} and R_g^{min} respectively. These quantities were calculated for all ligands in the N and Z sets, and the difference in maximum and minimum radius of gyration computed respectively for each ligand as $\Delta R_g^{min}(N–Z) = R_g^{min}(N) - R_g^{min}(Z)$ and $\Delta R_g^{max}(N–Z) = R_g^{max}(N) - R_g^{max}(Z)$. A positive value of ΔR_g^{min} or ΔR_g^{max} indicates that the N conformers are more extended than their corresponding Z conformers.

ROCS

The ROCS method [22] as implemented in the OpenEye suite was used. The ROCS method determines the maximum volume overlap of two molecules, modeled via Gaussians, using rigid-body superposition. We use the ComboScore scoring function in ROCS; this combines the ShapeTanimoto score, a quantitative measure of steric overlap of two molecules, with ColorScore, which represents the chemical functionalities calculated via the atomic charges assigned to the molecules. As the value of ShapeTanimoto and ColorScore ranges from 0 to 1, where 1 is maximum overlap and 0 is no overlap, ComboScore, which combines the two functions with equal weight, can vary from 0 to 2 [35].

Pharmacophore generation

MOE [23] was used to build pharmacophore queries. Four reference Type II ligands, binding to three different protein kinases, were selected in the study: **1** (PDB code 1IEP), **2** (1KV2), **3** (1UWH) and **4** (3CS9). The four protein/ligand complexes were superimposed using Needleman–Wunsch alignment [36] as implemented in MOE, and pharmacophoric features were added from common annotation points such as hydrogen bond donor/acceptor, hydrophobic, aromatic and excluded volume. The additional constraint of the presence of essential pharmacophoric features in the query was explored. A total of 21 queries were built and used to search the databases of Type I and II molecular conformations.

All screening processes were implemented into Pipeline Pilot [37] so that databases could be processed quickly and changes in parameters readily explored.

Analysis of screening

We define a number of measures used to assess the quality of screening for Type II ligands. The Type II retrieval ratio is defined as (*number of Type II molecules retrieved*)/(*total number of Type II molecules in the dataset*). The Type II/Type I retrieval ratio is defined as (*number of Type II molecules retrieved*)/(*number of Type I molecules retrieved*). Sensitivity (Se) [38] is defined in the context of in silico screening as the number of true positive (TP) compounds divided by the sum of TP and false negative (FN), ie. TP/(TP + FN). Specificity (Sp) is defined as number of true negative (TN) compounds divided by the sum of TN and false positives (FP), ie. TN/(TN + FP). Related to this is the receiver operating characteristic [21, 38, 39] (*roc*) curve; a *roc* curve is a plot of Se (the true positive rate) versus 1-Sp (the false positive rate). Such plots can be used to study the ability of screening protocols to distinguish active from inactive compounds. For a combined pharmacophore/ROCS search, values of 10 and 0 for pharmacophore matches and mismatches respectively were added to the ROCS score to calculate the final *roc* score.

Results

Common geometric features of Type II inhibitor binding modes

We have identified the crystal structures of 55 Type II inhibitor/protein kinase complexes based on the presence of a DFG-out loop conformation in the protein kinase (Online resource, Table 1S). These complexes involve 14 different protein kinases. Similarly, 83 Type I inhibitor/protein kinase structures were identified with DFG-in loop

conformations present (Table 2S). This comprises 29 distinct protein kinases, five of which are common to the Type II set. From overlay of the Type II inhibitor/protein kinase structures and in agreement with previous studies using smaller datasets [5, 8], four main loci of interaction with the protein kinase are apparent (Fig. 2): (1) *a hinge region binder* (HRB) group which occupies the ATP binding pocket; the scaffold usually consists of aromatic groups with side chains or hetero-aromatic rings capable of creating hydrogen bonds with the protein; (2) *a hydrophobic moiety* (HM), situated in the deep pocket exposed by the DFG-out (inactive) conformation. The HM of Type II inhibitors gives an advantage over Type I inhibitors, as it can be fine-tuned to improve protein kinase potency and selectivity. As a result, the size and structure of the HM was found to vary quite considerably over the set of crystallographic Type II inhibitor structures; (3) *a linker*, which connects the HM and the HRB, usually containing an aromatic scaffold which is used to modulate selectivity; (4) finally, between the linker and the HM, there must be a *hydrogen bond acceptor and/or donor functionality* (*HAHD*): this is often fulfilled by a urea functional group (e.g. **2** and **3**, Scheme 1) or an amide group (**1** and **4**, Scheme 1); however other functional groups [40] have successfully been designed such as benzoxazole or benzimidazole [41] for vascular endothelial growth factor-2 receptor (VEGFR2) tyrosine kinase inhibitors.

Strikingly, we observe a rather conserved relative orientation of HRB, linker and HM groups, forming a characteristic and well conserved V-like shape. We quantify this geometry by defining angle θ between the horizontal planes of the HM and HRB (Fig. 2). Over the 50 Type II inhibitors which possess all three main regions, θ is narrowly distributed (Fig. 3a), with a value of $121 \pm 8°$ (Table 1; Table 3S). This reflects the expected 120° geometry typical of a meta-substituted benzyl linker group. Where measurable, θ is found to be $135 \pm 28°$ ($n = 51$) in the Type I set. The range of proteins explored by these two analyses is approximately similar: 19 different kinases for Type I complexes as compared to 12 kinases for Type II complexes.

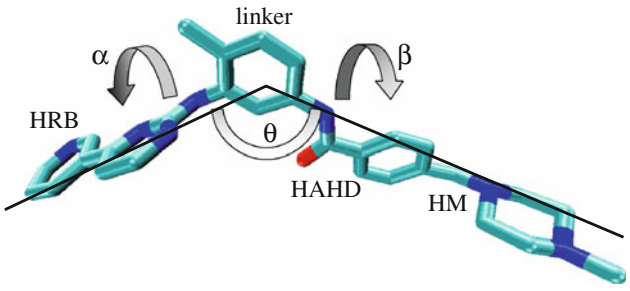

Fig. 2 The four main protein kinase binding components of a Type II ligand (HRB, linker, HAHD and HM); and definition of angle θ, and dihedral angles α and β, with the *black lines* lying in the plane of the specific components

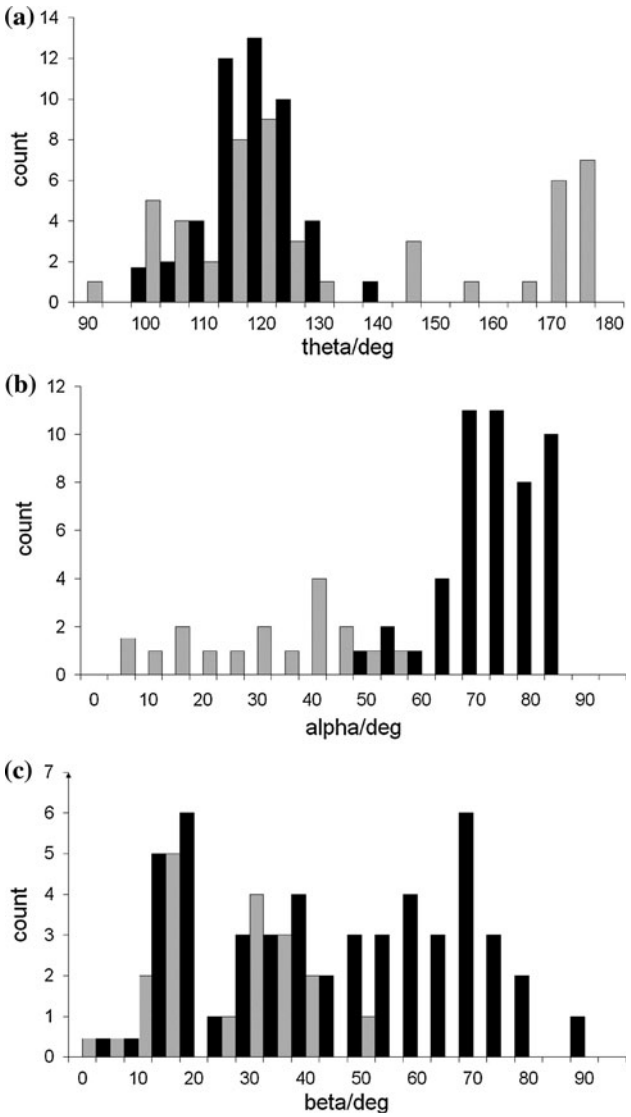

Fig. 3 Distribution of angles **a** θ, **b** α and **c** β, for Type I (*grey*) and Type II ligands (*black*)

Table 1 Average geometries for Type II inhibitor conformations (standard deviations in parentheses)

Coordinate	Average
θ	120.8 (7.9)
α	77.7 (8.1)
β	46.0 (23.6)
Asp381 H*N*···*O*=C ligand	3.00 (0.30)
Glu286 *Oδ*···*N*H ligand	3.03 (0.56)

Angles in deg and distances in Å

Less intuitive, however, is the conservation of dihedral angle α. This angle is defined between the planes formed

by the aromatic parts of the HRB and linker (Fig. 2). This angle has an average value of 78 ± 8° for Type II ligands (Table 1; Fig. 3b), quite distinct from Type I compounds (29 ± 17° for $n = 20$). Design strategies frequently seek to induce such a conformation, for example through introduction of a "magic methyl" group at the ortho substitution of the linker from the linker-HRB bond, in order to stagger the relative conformation of the linker and HRB [5]. However, the average conformation we observe from the crystal structures is not truly orthogonal [5], but appears tilted from 90°. This 78° average value of the torsion angle (Table 1) seems important to ensure the ligand curves from the HRB, with its specific hydrogen bonding requirements, around the protein backbone of residues 379–383 and towards the deep pocket (note that throughout this paper, we follow the residue numbering of c-Abl from PDB code 1IEP [16]).

By contrast, at the deep pocket, the torsion angle β between the planes of the linker and HM (Fig. 2) has a much larger standard deviation of 24°, around a mean value of 46° (Table 1; Fig. 3c). This might be expected given the HM of the inhibitors is used to fine tune specificity and potency to the range of deep pockets found in different protein kinases. The equivalent value in Type I compounds is 26 ± 14°, for the 21 compounds where this angle can be defined (Fig. 3c).

Across the set of Type II inhibitor complexes, we also observe conservation of the two key hydrogen bonds from the protein kinase to the ligands' urea/amide HAHD group. Firstly, the side chain of Glu286 from the αC helix makes a hydrogen bond with inhibitors' amide or urea group (Fig. 4); the average Glu286 Oδ···N ligand distance is 3.03 ± 0.56 Å (Table 1). Secondly, the backbone amide N of Asp381 of the DFG motif interacts with the amide/urea O of the ligand (Fig. 4); the average distance here is 3.00 ± 0.30 Å (Table 1). For both distances, the low value of standard deviation over the 55 structures implies that these hydrogen bonding interactions are rather strict requirements for Type II inhibitor binding.

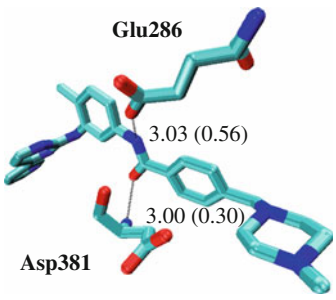

Fig. 4 Polar contacts between ligand amide group and residues Asp381 and Glu286. Average distances from crystallographic analysis in Å (standard deviations in *parentheses*)

Screening for Type II inhibitors

Given these conserved and characteristic features of Type II inhibitors, we here explore computational approaches to identify Type II compounds from a larger pool of compounds. We consider that the most appropriate and exacting decoys are Type I inhibitors, many of which are similar in size and composition to Type II molecules; for example compare **5–7** with **1–4** respectively (Scheme 1). For 83 Type I and 55 Type II inhibitors, conformational ensembles were generated using four different conformer generators: Macromodel [24], MOE [23], Omega [25] and SPE [26]. Furthermore, two different protonation strategies were explored, giving rise to the N (neutral) and Z (zwitterionic) sets (see Methods). We also group the ligands into chemistry-specific sets: (1) the *Urea* set, composed of 8 Type I and 12 Type II ligands, all possessing the urea chemical group between HM and linker; (2) the *Amide* set, containing 75 Type I and 31 Type II ligands, all with the amide moiety connecting HM and linker; and (3) the *Type II* set of 55 Type II compounds, comprising 12 urea-based, 31 amide-based and 12 other compounds.

Development of pharmacophore models

We first consider the development of a pharmacophore-based screen to discriminate Type II from Type I protein kinase inhibitors. Four known Type II protein kinase inhibitors, **1–4** (Scheme 1) were chosen for pharmacophore generation, using their crystallographic conformations from Protein Data Bank structures 1IEP, 1KV2, 1UWH and 3CS9 respectively. These four molecules have unrelated scaffolds, bind to three different protein kinases (c-Abl, p38 and B-Raf) and three of them, **1**, **3** and **4** are marketed.

A four-point Type II pharmacophore was initially explored; features were situated only on the linker and HM region, and consisted of: (1) on the linker, an oriented π-system, aromatic or hydrophobic feature; (2) at the centre of the HM region, an aromatic or hydrophobic feature; (3) on the N of the amide or urea group of **1–4**, a hydrogen bond donor feature; and (4) on the carbonyl O of the amide or urea group, a hydrogen bond acceptor feature. A number of pharmacophore queries were created using this model, varying in sphere volume of the features. However initial four-point pharmacophores did not filter out the majority of Type I molecules (data not shown).

Therefore, two additional pharmacophore points were added to the HRB area: (1) a hydrophobic/hydrogen bond acceptor feature situated close to the linker region; and (2) at the far end of the HRB, a hydrogen bond acceptor feature (Fig. 5). 21 variants of this six-point pharmacophore query were then explored (**Q1–Q21**) which varied in

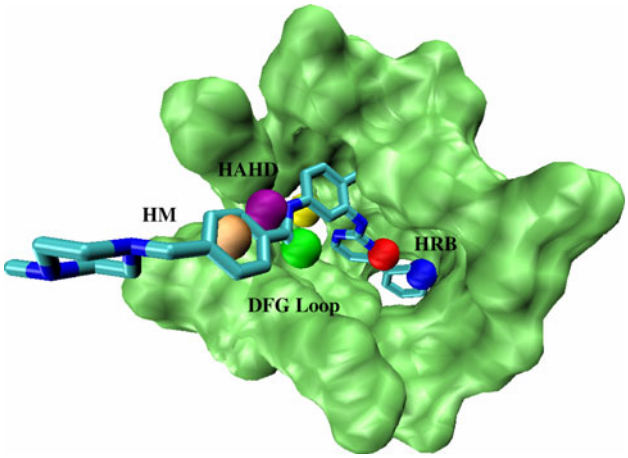

Fig. 5 Features of six-point pharmacophore: (1) hydrogen bond donor (*purple*); (2) aromatic/hydrophobic (*pink*); (3) π-ring normal centroid/aromatic/hydrophobic/hydrogen bond acceptor (*yellow*); (4) hydrogen bond acceptor (*green*); (5) hydrogen bond acceptor (*blue*); (6) hydrophobic/hydrogen bond acceptor (*red*). The green excluded volume refers to model **Q7**

(a) feature sphere diameter; (b) feature combinations, assigned as optional or essential to match; and (c) number of excluded volume constraints. The latter involves partial creation of an inverse picture of the protein via specifying regions of space forbidden to compounds. Inclusion of the following three receptor regions was found to be optimal: (1) residue Glu286; (2) residues in the DFG motif; and (3) residues in the hinge region (specifically residues 253, 269–271, 299, 313, 315–318, 321, 370, 380, 382).

Out of the 21 distinct queries, the best performing were **Q2**, **Q4**, and **Q7**. These share the same diameter of the six feature points (see Table 4S). However, they differed in that: **Q2** contained one grouped excluded volume in proximity to the hydrogen bond donor feature of HAHD and had three of its six features (on the HM, linker and HRB) deemed essential; **Q4** contained one grouped excluded volume constraint, based on the hinge region residues and had three of its six features (on the HM, linker and HRB) deemed essential; query **Q7** included all three grouped excluded volumes and had no features marked as essential (Fig. 5).

Pharmacophore-based screening: effect of ligand protonation state

We now turn to evaluate the ability of pharmacophores **Q2**, **Q4** and **Q7** to identify Type II molecules from the *Type II* set of 55 Type II inhibitors. Here, we also compare the use of the neutral (N) and zwitterion (Z) versions of the *Type II* set. Considering first the zwitterion set, the number of Type II molecules recovered varies from 53% using SPE to 82% using MOE (Table 2). Interestingly, SPE and MOE produce a comparable number of conformers per Type II compound, 479 and 510 respectively (Table 3); this is rather fewer than the 824 per ligand produced by Omega (Table 3). For the neutral *Type II* set, the proportion of Type II molecules retrieved is the same or improved in all cases relative to the Z set, regardless of conformer generator (Table 2). (The similarity of results for Z and N sets generated by SPE and Omega is not unexpected from their algorithms, which are essentially independent of protonation state.) The largest improvement is seen for Macromodel's generated ensembles, where the number of Type IIs retrieved on average using **Q2** increases from 67% for the Z set to 84% for the N set (Table 2). This does link with an increased number of unique conformers per molecule generated via Macromodel, by 76 conformers/molecule (Table 3).

Table 2 Comparison in Type II retrieval ratios (%) of pharmacophore screen from the zwitterion (Z) and neutral (N) versions of the *Type II* ligand set using different conformer generators

Query	Macromodel		MOE		Omega		SPE	
	N	Z	N	Z	N	Z	N	Z
Q2	83.6	67.3	81.8	81.8	78.2	78.2	72.7	70.9
Q4	69.1	60.0	67.3	63.6	74.5	72.7	58.2	58.2
Q7	67.3	56.4	65.5	61.8	69.1	67.3	54.5	52.7

Table 3 Number of conformers generated for the specific data sets, neutral (N) and zwitterion (Z)

	Type II (N)	*Type II* (Z)	Amide	Urea
Macromodel	31531 (573)	27345 (497)	51972 (490)	8198 (410)
MOE	28693 (522)	28101 (510)	48519 (458)	7320 (366)
Omega	45340 (824)	45340 (824)	88174 (832)	14867 (743)
SPE	26025 (473)	26327 (479)	62894 (593)	5455 (273)

The average number of conformers per ligand is given in parentheses

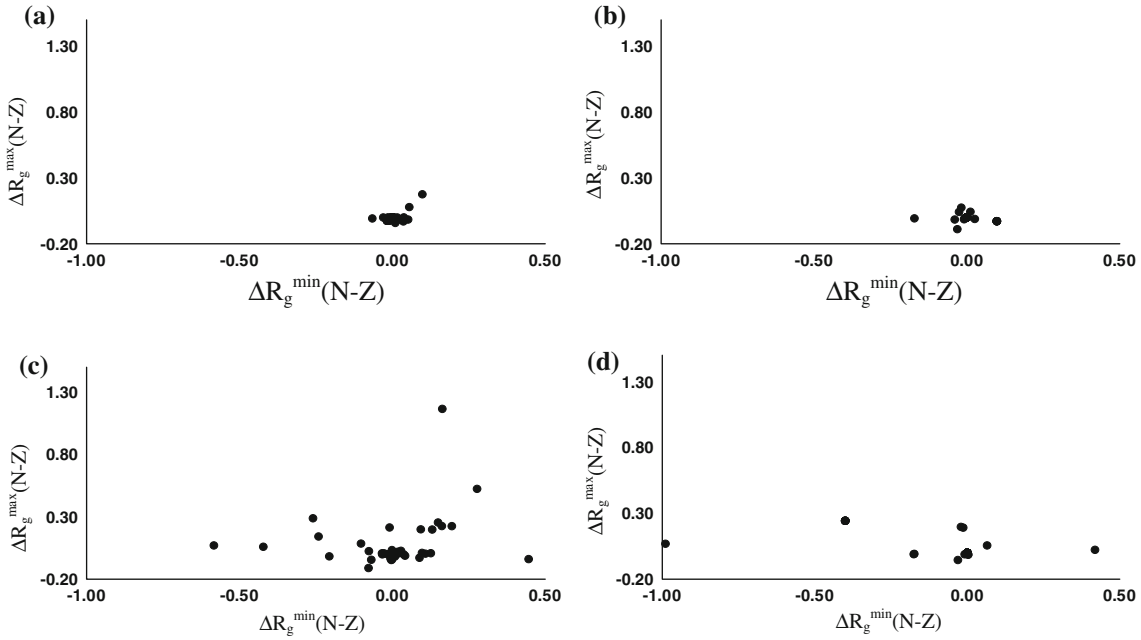

Fig. 6 Difference in maximum radius of gyration, ΔR_g^{max}(N–Z), versus difference in minimum radius of gyration, ΔR_g^{min}(N–Z), for ensembles of molecules generated using **a** SPE, **b** Omega, **c** Macromodel and **d** MOE

The radius of gyration is used to measure the geometric diversity of conformation [42]; here we use the difference in radius of gyration between N and Z conformer sets to evaluate the effect of charge on compactness of conformers. The generally positive ΔR_g^{max} values observed with Macromodel (Fig. 6c) suggest that this method samples more extended conformers for neutral versus zwitterionic conformers. ΔR_g^{min} appears to exhibit a spread across positive and negative values. For SPE and Omega, the spread observed for ΔR_g^{min} is close to zero as expected from their algorithms (Fig. 6a, b). For MOE, there is little difference in R_g^{max} for N and Z sets (Fig. 6d); however, there is a notable difference in ΔR_g^{min} for some compounds created by MOE.

Overall, the N set appears to provide a similar or slightly more diverse range of conformers relative to the Z set; this is in line with previous work [42]. Moreover, using the N version of the Type II set, the pharmacophores retrieve more Type II molecules on average (Table 2). In subsequent analyses, we employ the N set.

Pharmacophore-based screening: discrimination from Type I decoys

We next consider the ability of pharmacophores **Q2**, **Q4** and **Q7** to retrieve Type II inhibitors from ligand sets containing both Type II and Type I molecules. The Type I ligands are decoys and contain amide and urea chemistries. We consider first the *Amide* ligand set, which is the larger of the two sets, containing 31 Type II and 75 Type I molecules. The ratio of Type II/Type I molecules recovered via the pharmacophores ranges from 1.7 to 4.7 (Table 4). In particular, conformers retrieved using pharmacophore **Q7** appear effective in minimizing false positives (retrieved Type Is), with an average retrieval ratio of 3.8 compared to 1.8 for **Q2** and 2.8 for **Q4**. It appears that it is necessary to include all excluded volume restraints in the pharmacophore to effectively exclude Type I molecules. The most effective conformer generators for the *Amide* set appear to be Macromodel and to a lesser extent SPE, with consistently higher retrieval ratios than MOE

Table 4 Type II/Type I retrieval ratios for *Amide* and *Urea* sets using different conformer generators

Query	Macromodel		MOE		Omega		SPE	
	Amide	*Urea*	*Amide*	*Urea*	*Amide*	*Urea*	*Amide*	*Urea*
Q2	2.05	2.44	1.74	1.83	1.67	1.67	1.80	1.50
Q4	3.39	1.67	2.42	2.33	2.62	3.00	2.82	1.78
Q7	4.67	3.00	2.88	4.67	3.23	3.00	4.32	2.33

and Omega (Table 4). The best combinations are therefore found using **Q7** together with the Macromodel or SPE conformer generators (retrieval ratios of 4.7 and 4.3 respectively). For the **Q7**/Macromodel method, this in fact corresponds to recovery of 87% of Type II molecules versus 19% Type I amide-containing molecules (Table 5S).

We turn to consider the ability of **Q2**, **Q4** and **Q7** to retrieve Type II ligands from the *Urea* ligand set. Due to availability, this set contains only 12 Type II inhibitors (and 8 decoys), which inevitably limits the generality of conclusions drawn from analysis of the set. This said, as for the *Amide* set, pharmacophore **Q7** proves the most discriminatory, with an average Type II/Type I retrieval ratio across conformer generators of 3.2, relative to 2.0 for **Q2** and 2.2 for **Q4**. Interestingly, for the Ureas, the highest retrieval ratio is found using MOE, with a value of 4.7 is observed for **Q7**/MOE (Table 4). Underlying this, however, it appears that only 58% of Type IIs are retrieved, along with 12% of the decoys (Table 5S). In general, it seems discrimination of urea-based Type IIs is more difficult than for amides (although we note that the ureas are a smaller set): 92% of ureas are found with either **Q2**/Macromodel or **Q2**/MOE, but in addition, 38% and 50% Type Is respectively are also retrieved (Table 5S).

A useful summary of the effectiveness of the pharmacophore models in screening for Type IIs is obtained from consideration of selectivity (Se) and specificity (Sp). In the context of this work, selectivity is a measure of how well Type IIs are detected during screening (1 being the maximum value, see Methods). Specificity relates to how well Type I compounds are excluded by the screen (again, the maximum value is 1). In terms of pharmacophore, **Q2** and **Q4** exhibit the greatest selectivity (Table 6S), with Se values for the *Amide* set, averaged over conformer generator, of 0.91 and 0.89 (Table 7S). This compares with values of 0.85 for **Q7**. Conversely, **Q7** shows superior specificity in excluding Type I compounds, with values of 0.78, relative to 0.69 for **Q4** and 0.50 for **Q2** (Table 7S).

Roc scores provide a useful combined measure of selectivity and specificity, given by the area under the curve of a receiver operating characteristic plot (Table 7S; Table 5a). Indeed, averaged over conformer generator, **Q7** shows the highest *roc* score for the *Amide* set (0.80, Table 7S) relative to **Q2** (0.72) and **Q4** (0.69). Considering conformer generator, the highest *roc* score for the *Amide* set when averaged over pharmacophore is found for Macromodel with a value of 0.80 (Table 7S); this is followed by SPE (0.77) and then Omega (0.74) and MOE (0.73). For the smaller *Urea* set, *roc* scores indicate a better performance by Macromodel and Omega over SPE and MOE (Table 7S).

We note that despite the general success of the pharmacophore model, two Type II molecules from the *Amide* set were not picked up by any method (Table 8S): a nicotinamide derivative (2P2I) [43] and an Astex compound (1WBV) [44]. Also two Type IIs were not retrieved from the *Urea* set: a BIRB796 fragment (1KV1) [11] and 4-amino-furo[2,3-d]pyrimidine (1YWN) [45]. These Type II ligands are unable to adopt an overall V-shape due to (a) a direct covalent bond between the linker and pendant group ring systems (1WBV and 1YWN); (b) an ortho-substituted central linker (2P2I); and (c) an absent hinge binding moiety (1KV1). Conversely, all methods struggled to exclude a core of eight Type I molecules from the *Amide* set and one from the *Urea* set (Table 8S).

Shape-based screening using ROCS

The pharmacophore-based approaches applied above appear able to retrieve the majority of Type II molecules. Inclusion of increased excluded volume into the queries appears to improve specificity. Here, we explore an alternative approach to detecting Type II molecules, using ROCS [46] to match ligand shape/volume and chemistry. ROCS is capable of rapidly maximizing the overlap volumes of molecule pairs, modeling shape using atom-centred Gaussian functions. Here, this is used with the ComboScore scoring function to add chemical information (see Methods). We evaluate the ability of ROCS to discriminate Type II from Type I inhibitors. To generate shape queries for ROCS, the same four molecules as used for pharmacophore generation are used here, namely **1**–**4** (Scheme 1).

For the *Amide* set, molecule **4** performs best out of the four inhibitor-based shape queries, with the highest *roc* scores of 0.90–0.93 (Table 5b). This may stem from the more branched HM component of ligand **4**, mapping out the hydrophobic pocket to a greater degree than for example **1**. These high *roc* scores indicate ROCS to be quite discriminatory using compound **4**; indeed these scores appear competitive with values obtained from the pharmacophore approach, which has a maximum *roc* score of 0.84 for amides (Table 5a). For ROCS-based screening of the *Amide* set, the *roc* score did not vary by more than 0.08 across conformer generator (Table 5b).

For the *Urea* set, using compound **2** as the ROCS query gives the highest *roc* scores, with values of 0.94 using Macromodel and 0.96 using MOE (Table 5). The *roc* scores of 0.8–1.0 for screening the *Urea* set using ROCS (Table 5b) are higher than that found for the pharmacophores (0.6–0.8, Table 5a). Unsurprisingly, the best query ligand for screening ureas using ROCS, inhibitor **2**, is itself urea-based; it seems the additional conformational restriction arising from this functionality is important to take into

Table 5 *Roc* scores using (a) pharmacophores, (b) ROCS with different shape queries and (c) a combined pharmacophore and ROCS approach to screen *Amide* and *Urea* databases for Type II inhibitors

	Macromodel		MOE		Omega		SPE	
	Amide	*Urea*	*Amide*	*Urea*	*Amide*	*Urea*	*Amide*	*Urea*
(a) *Pharmacophore*								
Q2	0.73	0.77	0.69	0.71	0.68	0.67	0.71	0.63
Q4	0.82	0.67	0.75	0.67	0.76	0.75	0.79	0.65
Q7	0.84	0.75	0.76	0.73	0.77	0.75	0.81	0.67
(b) *ROCS*								
1 (1IEP)	0.81	0.79	0.79	0.81	0.82	0.71	0.74	0.56
2 (1KV2)	0.74	0.94	0.77	0.96	0.80	0.78	0.80	0.70
3 (1UWH)	0.80	0.88	0.85	0.87	0.84	0.88	0.86	0.81
4 (3CS9)	0.93	0.72	0.93	0.76	0.91	0.60	0.90	0.58
Consensus	0.90	0.88	0.91	0.92	0.90	0.89	0.90	0.83
(c) *Pharmacophore then ROCS*[a]								
Q2	0.82	0.85	0.89	0.91	0.88	0.88	0.85	0.92
Q4	0.82	0.90	0.88	1.00	0.83	0.78	0.83	0.88
Q7	0.85	0.94	0.87	1.00	0.78	0.78	0.82	0.93

[a] All three combined approaches use a consensus query with ROCS

account when screening for other urea-based inhibitors. Therefore, urea **3** also performs reasonably well in retrieving other ureas (minimum *roc* score of 0.81, Table 5), but amide queries **1** and **4** perform poorly in this across conformer generators (minimum *roc* score of 0.56, Table 5). To ensure a good screening performance for both linker functionalities and across conformer generators, the use of a consensus query for ROCS based on molecules **1**–**4** proved most effective, with *roc* scores ranging from 0.83 to 0.92 (Table 5b).

Screening using a pharmacophore and ROCS

In a final stage of evaluation, we combine pharmacophore-based and shape-based methods, using ROCS as a post-processing step to prior pharmacophore screening. As the most generally effective shaped-based screen, the consensus query was used for ROCS analysis. *Roc* scores were calculated in turn for each of the pharmacophore queries **Q2**, **Q4** and **Q7** in combination with ROCS (Table 5c).

In terms of discriminative identification of the Type II *Amide* set, the performance of solely ROCS using a consensus query is generally not improved upon by inclusion of a pharmacophore. For the case of **Q7**/Omega, the *roc* score in fact reduces from 0.90 to 0.78 (Table 5). The least deterioration in performance on including the pharmacophore is found using the MOE conformer set (0.02–0.04). Interestingly, for the smaller *Urea* set, the ability to detect true Type IIs is generally improved by the combination of pharmacophore with ROCS. The exception is Omega, where the *roc* score is reduced from 0.90 (ROCS only) to 0.78–0.88 (ROCS with **Q2**–**Q7**, Table 5c). High *roc* scores are particularly found for **Q7**, and notably, for MOE, a *roc* score of unity is obtained for the *Urea* set (Table 5), indicating the identification of all 12 true Type IIs and rejection of all 8 decoys.

In broad terms, when using the combined pharmacophore/ROCS approach, all four conformer generators perform comparably based on *roc* scores (0.8–1.0).

Discussion and conclusions

We have performed a geometric analysis of 55 Type II inhibitors and find they adopt a distinctive twisted V-shape, characterised by a mean angle θ for HRB-linker-HM of $121 \pm 8°$ and dihedral angle α of $78 \pm 8°$ between HRB and linker planes; the less conserved deep pocket interactions are reflected by a more variable linker-HM torsion angle β of mean $46 \pm 24°$. The α angle orientation of Type II compounds is quite distinct from Type I compounds, differing by $\sim 50°$ (α of $29 \pm 17°$ for 20 Type Is). Additionally, the Type II inhibitors characteristically hydrogen bond to Asp381 and Glu286. We note that the distinct α/θ orientation is witnessed in the most recently solved Type II/kinase crystals structures; for example new structures not included in our data set involve ligand complexes with c-Src [48], p38 MAP kinase [49] and B-Raf [50]; in these structures, the ligands adopt an angle α of 73°, 62° and 81° respectively, as well as forming good hydrogen bonds with Asp381 and Glu286 (Table 9S). Caution should be exercised, however, as exceptions to this shape can be found: for

example, the bound pose of Type II compound BIRB796 in pyk2 has an α value is 46° [51]. This is due in large part to an absence of interaction between the morpholine substituent of BIRB796 and the kinase hinge region.

We have sought to translate this information on typical Type II pose into pharmacophore-based and shape-based screens for Type II inhibitors, using Type I inhibitors as decoys. The most effective pharmacophores contain six features; the inclusion of excluded volumes (**Q7**) was also found to be important, to ensure exclusion of decoys during screening.

Qualitative Type II pharmacophores have been proposed previously: for example, a descriptive seven-feature model by Okram et al. [15] was used to design new Type II inhibitors for Abl. Their model had a hydrogen bond acceptor/donor pair and hinge binding moiety, a hydrophobic motif for the linker and HM parts, and a hydrogen bond acceptor/donor pair between linker and HM. A simpler four-feature model was used to discuss Type II inhibitors by Backes et al. [5], resolving ligands into hinge, DFG, Glu-Lys and deep pocket binding components. Quantitative pharmacophore models were developed by Xie et al. [14], specifically for Type I and Type II Tie2 protein kinase inhibitors (Tie2 is closely related to VEGFR-2). Here, a five-feature model was found sufficient to explain Type II Tie2 inhibition, with the additional use of two excluded volume constraints (in the HM region). The five features were two hydrogen bond donors (one in the hinge and one in the linker/HM junction), two general hydrophobic features (at linker and HM) and one hydrophobic aromatic moiety (at the hinge). Using our general six-point pharmacophore model, which also includes three excluded volume constraints (**Q7**), we obtain *roc* scores of 0.67–0.84 (Table 5a), indicating that this method exhibits discrimination for Type II inhibitors.

For shape-based screening, we applied the ROCS method. Consensus scoring using four distinct ligand queries, two urea-based and two amide-based, from complexes with three different protein kinases produced the most effective results from ROCS; the approach was as good, and in several cases, better than the pharmacophore approach. *Roc* scores here reach 0.93 for the *Amide* set and 0.96 for the *Urea* set (Table 5b). Only for detection of urea-based Type II inhibitors, of which there were only 12 in our test set, was there a small but measurable benefit by combining pharmacophore and ROCS methods as a two-stage screen. We note that the ComboScore function used with ROCS includes both shape and chemical information (the latter via "colour"—see "Methods"); and therefore, in a sense, coloured atoms mimic some features of the pharmacophore model. Consequently, it is not entirely unexpected that the benefits of combining both pharmacophores and ROCS (colour and shape) appear limited.

Finally, we consider the effect of conformer generator. In general, the dependence of pharmacophore-based and ROCS-based screens on conformer generator was relatively weak. For pharmacophore-based screening of *Amide* and *Urea* sets, Macromodel appeared the most effective generator. We note that for known actives recovered by this approach, conformers selected are typically in reasonable agreement with crystallographic conformations, as illustrated for poses of **3** and **1** (Fig. 7a, b); however alternative conformers, whilst still retaining an overall V-shape, can also match the pharmacophore (Fig. 7c).

For the ROCS shape-based approach, the performance of Macromodel, SPE, Omega and MOE was similar for amide-based ligands. For urea-based compounds, there was a little more variation, with MOE and Macromodel performing most satisfactorily. Recently, the ability of the four search algorithms to sample conformational space was compared [47]. The number of molecules was computed for which a particular method failed to produce a conformation within 10 kcal/mol of the global minimum. Interestingly, both Macromodel and Omega produced over 20 failures (out of 59 molecules). MOE had 10 failures and SPE produced fewer than 5. For the tighter cut-off of 5 kcal/mol, Omega performed better than Macromodel. The study also noted that without conformational boosting, SPE tended to produce a rather compact ensemble of

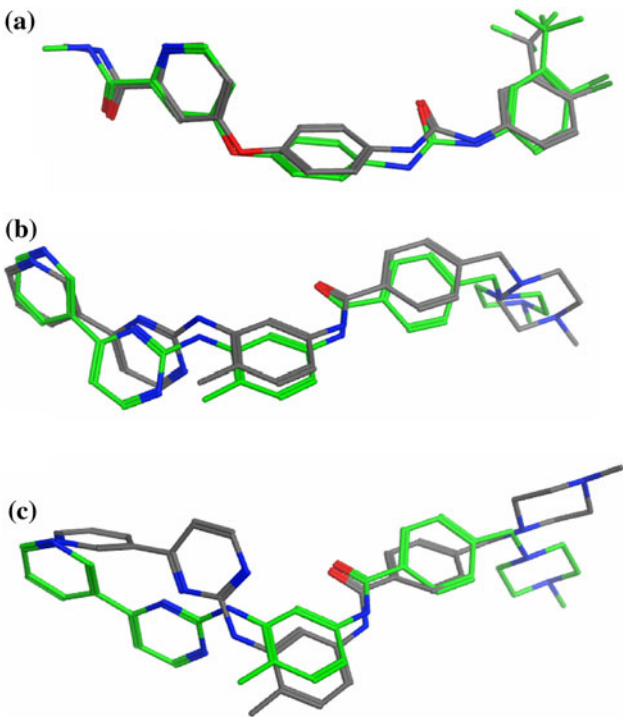

Fig. 7 Crystallographic (*green*) and Macromodel conformations selected from screening with pharmacophore **Q7** (*grey*), for **a** ligand **3** and **b**, **c** two alternative conformations of ligand **1**. Crystal structures are PDB codes 2BAK and 1IEP respectively

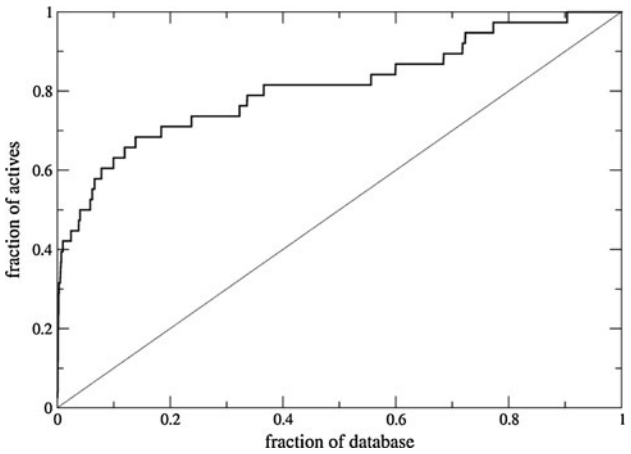

Fig. 8 Enrichment found from virtual screen of the DUD database (seeded with known Type II inhibitors) using a **Q7**/ROCS (consensus) screen

conformations. For MOE, Macromodel and Omega, there was found a bias towards more extended conformations, which should suit the generation of the poses required by Type II inhibitor binding modes.

We have shown that the shape-based and pharmacophore-based screening protocols introduced here distinguish Type II from Type I kinase inhibitors. However, in the broader context of large virtual screens, these approaches must also be able to discriminate actives from inactives in virtual screening studies. To demonstrate this, we have assessed the ability of the pharmacophore search and ROCS/consensus protocols to retrieve known Type II ligands from a modified version of the Directory of Useful Decoys (DUD) database [52, 53]. This database of over 104,000 compounds is tailored for assessment of ligand-based virtual screening, containing actives and decoys for 40 different protein targets. Macromodel was used to generate all conformers (1,000 per compound, see Methods). The 55 Type II compounds were used as positive hits and the DUD database of compounds as negative hits to calculate statistical measures. For the screen, we use the combination of a pharmacophore search using **Q7** followed by ROCS, where ROCS uses a consensus query. Despite the small number of actives used to validate the approach, the enrichment factors at 1%, 5% and 10% gave encouraging results, with values of 42%, 50% and 63% respectively (Fig. 8). The associated *roc* score was 0.81. The combined pharmacophore/ROCS screen was able to remove 93% of the compounds of the DUD database while keeping 70% of the Type II compounds.

In conclusion, our study suggests that ligand-based screening approaches can be effective for detecting Type II protein kinase inhibitors. Shape-based screening using ROCS with a consensus query performs at least as well as pharmacophore filters. These findings, based on screening ligands with neutral titratable groups, are found not to be strongly dependent on conformer generator. The in silico approaches we have explored here are relevant to screening corporate or other large virtual screening databases, as most of the conformer generators produce around 500 or fewer conformations per ligand (Table 3). Our approach is ligand-based; this complements receptor-based screening methods, including the DOLPHIN technique of Kurafeva and Abagyan [6], which is useful when only DFG-in kinase structures are available. Our hope is that this ligand-based approach, which has already shown promise in selecting known Type II kinase inhibitors from the large, diverse DUD database, will prove a valuable tool in the pursuit of new, potent and selective inhibitors of important protein kinase targets.

Acknowledgments This work was funded by the Biotechnology and Biological Sciences Research Council and Johnson & Johnson Pharmaceutical Research & Development. The authors would like to thank Dr. Trevor Howe and Dr. Berthold Wroblowski for their valuable comments; and Andrew Henry from Chemical Computing Group for his support in MOE scripting.

References

1. Zhang JM, Yang PL, Gray NS (2009) Nat Rev Cancer 9:28
2. Noble MEM, Endicott JA, Johnson LN (2004) Science 303:1800
3. Hanks SK, Quinn AM, Hunter T (1988) Science 241:42
4. Scapin G (2002) Drug Discov Today 7:601
5. Backes AC, Zech B, Felber B, Klebl B, Muller G (2008) Expert Opin Drug Discov 3:1427
6. Kufareva I, Abagyan R (2008) J Med Chem 51:7921
7. Backes AC, Zech B, Felber B, Klebl B, Muller G (2008) Expert Opin Drug Discov 3:1409
8. Liu Y, Gray NS (2006) Nat Chem Biol 2:358
9. Seeliger MA, Ranjitkar P, Kasap C, Shan YB, Shaw DE, Shah NP, Kuriyan J, Maly DJ (2009) Cancer Res 69:2384
10. Neumann L, Ritscher A, Muller G, Hafenbradl D (2009) J Comp Aided Mol Des 23:501
11. Pargellis C, Tong L, Churchill L, Cirillo PF, Gilmore T, Graham AG, Grob PM, Hickey ER, Moss N, Pav S, Regan J (2002) Nat Struct Biol 9:268
12. Zuccotto F, Ardini E, Casale E, Angiolini M (2010) J Med Chem 53:2681
13. McGregor MJ (2007) J Chem Inf Modell 47:2374
14. Xie QQ, Xie HZ, Ren JX, Li LL, Yang SY (2009) J Mol Graph Modell 27:751
15. Okram B, Nagle A, Adrian FJ, Lee C, Ren P, Wang X, Sim T, Xie YP, Wang X, Xia G, Spraggon G, Warmuth M, Liu Y, Gray NS (2006) Chem Biol 13:779
16. Nagar B, Bornmann WG, Pellicena P, Schindler T, Veach DR, Miller WT, Clarkson B, Kuriyan J (2002) Cancer Res 62:4236
17. Wan PTC, Garnett MJ, Roe SM, Lee S, Niculescu-Duvaz D, Good VM, Jones CM, Marshall CJ, Springer CJ, Barford D, Marais R (2004) Cell 116:855
18. Weisberg E, Manley PW, Breitenstein W, Bruggen J, Cowan-Jacob SW, Ray A, Huntly B, Fabbro D, Fendrich G, Hall-Meyers E, Kung AL, Mestan J, Daley GQ, Callahan L, Catley L, Cavazza C, Mohammed A, Neuberg D, Wright RD, Gilliland DG, Griffin JD (2005) Cancer Cell 7:129

19. Deak HL, Newcomb JR, Nunes JJ, Boucher C, Cheng AC, DiMauro EF, Epstein LF, Gallant P, Hodous BL, Huang X, Lee JH, Patel VF, Schneider S, Turci SM, Zhu XT (2008) Bioorg Med Chem Lett 18:1172
20. Araujo J, Mathew R, Armstrong AJ, Braud EL, Posadas E, Lonberg M, Gallick G, Trudel GC, Paliwal P, Logothetis CJ (2009) EJC Suppl 7:415
21. Oslob JD, Romanowski MJ, Allen DA, Baskaran S, Bui M, Elling RA, Flanagan WM, Fung AD, Hanan EJ, Harris S, Heumann SA, Hoch U, Jacobs JW, Lam J, Lawrence CE, McDowell RS, Nannini MA, Shen W, Silverman JA, Sopko MM, Tangonan BT, Teague J, Yoburn JC, Yu CH, Zhong M, Zimmerman KM, O'Brien T, Lew W (2008) Bioorg Med Chem Lett 18:4880
22. Rush TS, Grant JA, Mosyak L, Nicholls A (2005) J Med Chem 48:1489
23. Chemical Computing Group, Montreal, QC, Canada, 2003
24. Schrodinger; Schrodinger LLC (2005). http://www.schrodinger.com.
25. Omega; OpenEye Scientific Software (1997). http://www.eyesopen.com/.
26. SPE, Johnson and Johnson (2009)
27. Agrafiotis DK, Gibbs A, Zhu FQ, Izrailev S, Martin E (2006) Aust J Chem 59:874
28. Halgren TA (1999) J Comput Chem 20:720
29. Halgren TA (1996) J Comput Chem 17:490
30. Halgren TA (1996) J Comput Chem 17:520
31. Halgren TA (1996) J Comput Chem 17:553
32. Halgren TA, Nachbar RB (1996) J Comput Chem 17:587
33. Halgren TA (1996) J Comput Chem 17:616
34. Tresadern G, Agrafiotis DK (2009) J Chem Inf Modell 49:2786
35. Kirchmair J, Distinto S, Markt P, Schuster D, Spitzer GM, Liedl KR, Wolber G (2009) J Chem Inf Modell 49:678
36. Needleman SB, Wunsch CD (1970) J Mol Biol 48:443
37. Pipeline Pilot, Accelrys, Inc., San Diego, USA, 2010
38. Kirchmair J, Ristic S, Eder K, Markt P, Wolber G, Laggner C, Langer T (2007) J Chem Inf Modell 47:2182
39. Gribskov M, Robinson NL (1996) Comput Chem 20:25
40. O'Hare T, Shakespeare WC, Zhu XT, Eide CA, Rivera VM, Wang F, Adrian LT, Zhou TJ, Huang WS, Xu QH, Metcalf CA, Tyner JW, Loriaux MM, Corbin AS, Wardwell S, Ning YY, Keats JA, Wang YH, Sundaramoorthi R, Thomas M, Zhou D, Snodgrass J, Commodore L, Sawyer TK, Dalgarno DC, Deininger MWN, Druker BJ, Clackson T (2009) Cancer Cell 16:401
41. Potashman MH, Bready J, Coxon A, DeMelfi TM, DiPietro L, Doerr N, Elbaum D, Estrada J, Gallan P, Germain J, Gu Y, Harmange JC, Kaufman SA, Kendall R, Kim JL, Kumar GN, Long AM, Neervannan S, Patel VF, Polverino A, Rose P, van der Plas S, Whittington D, Zanon R, Zhao HL (2007) J Med Chem 50:4351
42. Bonnet P, Agrafiotis DK, Zhu FQ, Martin E (2009) J Chem Inf Modell 49:2242
43. Hodous BL, Geuns-Meyer SD, Hughes PE, Albrecht BK, Bellon S, Bready J, Caenepeel S, Cee VJ, Chaffee SC, Coxon A, Emery M, Fretland J, Gallant P, Gu Y, Hoffman D, Johnson RE, Kendall R, Kim JL, Long AM, Morrison M, Olivieri PR, Patel VF, Polverino A, Rose P, Tempest P, Wang L, Whittington DA, Zhao HL (2007) J Med Chem 50:611
44. Gill AL, Frederickson M, Cleasby A, Woodhead SJ, Carr MG, Woodhead AJ, Walker MT, Congreve MS, Devine LA, Tisi D, O'Reilly M, Seavers LCA, Davis DJ, Curry J, Anthony R, Padova A, Murray CW, Carr RAE, Jhoti H (2005) J Med Chem 48:414
45. Miyazaki Y, Matsunaga S, Tang J, Maeda Y, Nakano M, Philippe RJ, Shibahara M, Liu W, Sato H, Wang LP, Nolte RT (2005) Bioorg Med Chem Lett 15:2203
46. Grant JA, Gallardo MA, Pickup BT (1996) J Comput Chem 17:1653
47. Agrafiotis DK, Gibbs AC, Zhu FQ, Izrailev S, Martin E (2007) J Chem Inf Modell 47:1067
48. Getlik M, Gruêtter C, Simard JR, Kluêter S, Rabiller M, Rode HB, Robubi A, Rauh D (2009) J Med Chem 52:3915
49. Simard JR, Getlik Mê, Gruêtter C, Pawar V, Wulfert S, Rabiller M, Rauh D (2009) J Am Chem Soc 131:13286
50. Berger DM, Torres N, Dutia M, Powell D, Ciszewski G, Gopalsamy A, Levin JI, Kim KH, Xu W, Wilhelm J, Hu Y, Collins K, Feldberg L, Kim S, Frommer E, Wojciechowicz D, Mallon R (2009) Bioorg Med Chem Lett 19:6519
51. Han S, Mistry A, Chang JS, Cunningham D, Griffor M, Bonnette PC, Wang H, Chrunyk BA, Aspnes GE, Walker DP, Brosius AD, Buckbinder L (2009) J Bio Chem 21:13193
52. Huang N, Shoichet BK, Irwin JJ (2006) J Med Chem 49:6789
53. Jahn A, Hinselmann G, Fechner N, Zell A (2009) J Cheminform 1:14